RNA methyltransferase NSUN2 enhances vasculogenic mimicry and malignant progression of cervical cancer through upregulation of MMP-9

JUN LUO[1], GUANG LI[2], MEI YE[3], XIAOQING XU[1], MENGWEN QI[1], JIAN HUANG[4], KONG SHAN[2], LILI QU[1] and HENGCHUAN SHI[2]

[1]Reproductive Testing Quality Control Department of Central Laboratory, Jiangsu Health Vocational College, Nanjing, Jiangsu 211800, P.R. China; [2]Department of Laboratory Medicine, Geriatric Hospital of Nanjing Medical University: Jiangsu Province Geriatric Hospital, Nanjing, Jiangsu 212008, P.R. China; [3]Department of Gynecology, Nanjing Jiangning District Women and Children's Healthcare Hospital, Nanjing, P.R. China; [4]Key Laboratory of Systems Biomedicine (Ministry of Education), Shanghai Center for Systems Biomedicine, Shanghai Jiao Tong University, Shanghai 200241, P.R. China

Received November 28, 2024; Accepted November 24, 2025

DOI: 10.3892/ol.2026.15518

Abstract. Vasculogenic mimicry (VM), which creates an endothelium-independent tumor microcirculation, is associated with tumor metastasis and drug resistance, which are key challenges in the clinical treatment of cervical cancer (CC). The malignant progression of a variety of tumors is supported by the 5-methylcytidine (m^5C) modification of RNA. In the present study, potential relationships between VM formation and the m^5C modification in CC were investigated. Immunohistochemistry of CC tissues and a tissue microarray revealed that VM is prevalent in CC tissues but not in paracancerous tissues, and VM formation is associated with a poor prognosis in CC. Matrix metalloproteinase-9 (MMP-9) is highly expressed in CC tissues and in cell lines exposed to hypoxia. Using dot blotting and methylated RNA immunoprecipitation analyses, the m^5C modification was shown to be enriched in bulk RNA and in *MMP-9* mRNA isolated from VM-competent cultured CC cells. The NOP2/Sun RNA methyltransferase 2 (NSUN2) was highly expressed in CC tissues and cells and its expression was associated with poor prognosis in CC. Genetic interference with NSUN2 expression decreased VM formation in CC cells and it led to lower MMP-9 expression, suggesting that NSUN2 stabilizes *MMP-9* mRNA. This model, in which NSUN2 enhances VM by increasing MMP-9 expression, identified novel potential markers for early diagnosis of CC and potential therapeutic targets in the future.

Correspondence to: Professor Hengchuan Shi, Department of Laboratory Medicine, Geriatric Hospital of Nanjing Medical University: Jiangsu Province Geriatric Hospital, 65 Jiangsu Road, Nanjing, Jiangsu 212008, P.R. China
E-mail: njchinachuan@163.com

Abbreviations: CC, cervical cancer; CSC, cancer stem cells; CaSki, human cervical cancer cell line with intestinal metastasis; C33A, human cervical cancer cell line; DEPC, diethylpyrocarbonate; TRDMT1, transfer RNA aspartic acid methyltransferase 1; EET, epithelial-endothelial transformation; ECM, extracellular matrix; FBS, fetal bovine serum; HaCaT, human skin keratinocytes cell line; HeLa, human cervical cancer cell line; HT-3, human cervical cancer cell line; m^5C, 5-methylcytidine; MMP-9, matrix metalloproteinase 9; NSUN2, NOP2/Sun RNA methyltransferase 2; TCGA, The Cancer Genome Atlas; VM, vasculogenic mimicry; Sox2, SRY-box transcription factor 2; SiHa, human cervical squamous cell line

Key words: vasculogenic mimicry, NSUN2, MMP-9, cervical cancer

Introduction

Cervical cancer (CC) is the fourth most common cancer among women, with an incidence rate of ~10.9 per 100,000 in China (1). In recent years, methods of prevention, diagnosis and treatment of CC have improved notably, but metastasis and drug resistance remain key causes of CC treatment failure (2-5). Therefore, clarification of the mechanisms of development of CC remains a key research goal so that diagnostic and treatment strategies can be potentially enhanced in order to improve clinical outcomes for patients with CC.

A potentially key mechanism in this context involves the concept of Vasculogenic mimicry (VM), which was first proposed by Maniotis *et al* (6) in 1999 in a study of uveal melanoma. VM leads to the development of an endothelium-independent vascular system (7) in which a microcirculatory system is formed by tumor cells themselves under a hypoxic environment (8). The main process of formation of this system involves cancer stem cells (CSC) undergoing epithelial-endothelial transformation (EET). The resulting endothelial cells generate a duct structure due to remodeling of the extracellular matrix (ECM) and they ultimately fuse into vessels. This process is favored in the hypoxic microenvironment, where highly differentiated tumor cells gradually transform into lower-differentiated CSC with high

differentiation potential; notably, these CSC have a decreased sensitivity to chemotherapy agents and an increased susceptibility to the development of drug resistance (9-13). The tube formed by CSC with partial endothelial properties eventually fuses with endothelium-dependent microvessels to transport oxygen and nutrients to hypoxic regions of tumors.

The lack of endothelial cell coverage within the VM channel means that the tumor cells are directly exposed to the blood. This situation increases the likelihood that shed tumor cells will metastasize through the bloodstream, leading to early tumor metastasis (14-18). Therefore, VM is a key factor associated with increased metastasis and drug resistance and it has been reported to be associated with the occurrence, development and poor prognosis of multiple types of cancer, including breast (19), colorectal (20), prostate (21), hepatocellular (22), lung (23), ovarian (24), gastric (25) and bladder (26) cancer types.

Detailed molecular mechanisms underlying VM, particularly in CC, require further exploration; however, several molecular factors have been implicated in this process. For example, enzymes in the matrix metalloproteinase (MMP) family have been identified as being involved in VM due to their activities in the remodeling of the ECM (27,28).

Another potential molecular factor is the modification of RNA by the formation of 5-methylcytosine (m^5C) by methyltransferases. This change is a dynamic, reversible and widely distributed epigenetic modification (29) that serves a variety of biological functions (30,31). Notably in the context of VM, the levels of m^5C have been identified to increase in the hypoxic tumor microenvironment, where the modification promotes tumor growth, migration, angiogenesis and drug resistance. In particular, the NOP2/Sun RNA methyltransferase 2 (NSUN2) has been reported to be a key cancer-associated methyltransferase of this modification (32-34). Certain studies have explored roles for NSUN2 in CC (35,36); however, whether NSUN2 promotes the malignant progression of CC by enhancing VM in the hypoxic tumor microenvironment remains to be elucidated.

In the present study, bioinformatics and whole-slide scanning of immunohistochemical images were combined to investigate the association of VM with prognosis in CC. The present study also used bioinformatics and expression assays to demonstrate that MMP-9 may be particularly key in VM formation in CC. In order to study the mechanisms leading to increased expression levels of MMP-9, the m^5C modification of total RNA in CC was first quantified under hypoxic conditions using dot blot assay. Subsequently, the protein expression levels of NSUN2 was examined in hypoxia-induced VM-competent CC cells via western blot. Finally, a RNA stability and methylated-RNA immunoprecipitation assays were employed to study the physical and functional relationship between NSUN2 and *MMP-9* mRNA.

Patients and methods

Clinical tissue specimens. In the present study, 44 CC tissue samples and paired adjacent normal tissue samples were obtained during surgeries (May to August 2024) performed at the Jiangsu Province Geriatric Hospital, which is affiliated with Nanjing Medical University (Nanjing, China). The cohort consisted entirely of female patients, with a median age of 52 years (range, 42-68 years). For each patient, one sample of tumor tissue and one sample of histologically normal adjacent cervical tissue (obtained ≥3 cm from the tumor margin) were collected intraoperatively. The diagnosis of CC and the state of paracancerous tissues were confirmed by pathological evidence. All samples were immediately snap-frozen in liquid nitrogen and stored at -80˚C for at least 72 h prior to analysis. Patient inclusion criteria were as follows: i) Histopathologically confirmed primary cervical carcinoma; ii) scheduled for curative-intent surgery; iii) no prior radiotherapy, chemotherapy, or other anticancer treatments; and iv) provision of written informed consent for the use of resected tissue for research. Patient exclusion criteria included: i) A history of any other malignant tumor; ii) evidence of distant metastasis at presentation; iii) receipt of neoadjuvant therapy; and iv) insufficient quantity or poor quality of paired tissue samples as confirmed by pathological review. The present study was approved by the Ethics Committee of the Jiangsu Province Geriatric Hospital [approval no. (2024) Court Ethics Opinion No. 028-1] and written informed consent was obtained from all participants.

Cell culture and transfection. Normal cervical cells [human skin keratinocytes cell line (HaCaT; cat. no. TCH-C388; Haixing Biosciences Co., Ltd.; https://www.hycyte.com/sys-pd/133.html)] and CC cell lines [human cervical cancer cell line (HeLa; cat. no. TCH-C193; Haixing Biosciences Co., Ltd.; https://www.hycyte.com/sys-pd/65.html), human cervical squamous cell line (SiHa; cat. no. TCH-C326; Haixing Biosciences Co., Ltd.; https://www.hycyte.com/sys-pd/70.html), human CC cell line with intestinal metastasis (CaSki; cat. no. TCH-C145; Haixing Biosciences Co., Ltd.; https://www.hycyte.com/sys-pd/119.html), human CC cell line (C33A; cat. no. TCH-C143; Haixing Biosciences Co., Ltd.; https://www.hycyte.com/sys-pd/134.html) and human CC cell line (HT-3; cat. no. CL-0630; Wuhan Punoise Life Technology Co., Ltd.; https://www.procell.com.cn/p/ht-3-cl-0630-72192) were cultured in DMEM supplemented with 10% fetal bovine serum (FBS) purchased from Inner Mongolia Opcel Biotechnology Co., Ltd. (https://www.nmjyk.com/?tnxq/169.html) and penicillin/streptomycin (100 U/ml) in an incubator at 37˚C with 5% CO_2. Furthermore, cellular hypoxia was induced by exposing the cells to an atmosphere of 5% CO_2 and 0.1% O_2 for durations of 24, 48 and 72 h. All cell lines were free of mycoplasma. The cell lines used were authenticated using short tandem repeat analysis.

Lipofectamine® 2000 (Invitrogen; Thermo Fisher Scientific, Inc.) was used for transfection of cells with short hairpin RNA (shRNA) plasmid (10 μg; 1 μg/μl) and DNA transfection reagent (Roche Diagnostics) was used for transfection of cells with overexpression plasmids (4 μg; 1 μg/μl). Cells that were cultured to 50-70% confluence in 6-well plates were transfected according to the manufacturer's instructions in a 37˚C incubator. For shRNA plasmid transfection, the medium was changed 6 h after transfection, but the medium was not changed for overexpression plasmid transfections. RNA was collected 24 h after transfection and protein was collected 48 h after transfection.

Construction of plasmids and interference sequences. The *NSUN2*-targeting shRNA plasmid was purchased from

GeneCopoeia (cat. no. CSHCTR001-CU6; GeneCopoeia, Inc.) and its sequences were as follows: shNUSN2-1, 5'-CCCGGC CACTTTAAGAATTAC-3'; shNUSN2-2, 5'-CCTCATCAT AAGATCTTAGAT-3'; and shNSUN2-3, 5'-GCGATGCCT TAGGATATTACC-3'. The negative control sequence was 5'-GCTTCGCGCCGTAGTCTTA-3'.

The full lengths of the human *MMP-9* (NM_004994.3) and *NSUN2* (NM_017755) open-reading frames, as well as the full length open-reading frame of *GAPDH*, were cloned into the plasmid cloning DNA3.1(+) vector (cat. no. V80020; Invitrogen; Thermo Fisher Scientific, Inc.).

DNA and RNA extraction and reverse transcription-quantitative PCR (RT-qPCR). Plasmids containing the *NSUN2* and *MMP-9* sequences were extracted from *E. coli* DH5α using the Endo-free Plasmid Mini Kit II (Omega Bio-Tek Inc.) according to the manufacturer's instructions. Total RNA was extracted from CC cell lines or frozen tissue samples using TRIzol® reagent (Invitrogen; Thermo Fisher Scientific, Inc.) according to the manufacturer's protocol. RNA was reverse transcribed into cDNA using the PrimeScript™ RT reagent Kit (Perfect Real Time) Kit (cat. no. RR037A; Takara Bio, Inc.) according to the manufacturer's protocol and the DNA was stored at -20˚C. Quantitative PCR was performed on an ABI StepOne Plus Real-Time PCR System (Applied Biosystems; Thermo Fisher Scientific, Inc.) with three replicates for each sample, using TB Green® Premix Ex Taq™ (Tli RNaseH Plus) (cat. no. RR420A; Takara Bio Inc.). The thermal cycling profile was as follows: Initial denaturation at 95˚C for 30 sec, 40 cycles of denaturation at 95˚C for 5 sec, followed by combined annealing/extension at 60˚C for 30-34 sec (fluorescence data collection was performed at this step). Melt curve analysis was performed from 60-95˚C with a continuous fluorescence measurement at a ramp rate of 0.3˚C per sec. qPCR data were analyzed using the comparative Cq ($2^{-\Delta\Delta Cq}$) method (37). The primer sequences used were as follows: *NSUN2* F, 5'-GAA CTTGCCTGGCACACAAAT-3' and R, 5'-TGCTAACAG CTTCTTGACGACTA-3'; *MMP-9* F, 5'-GGGACGCAGACA TCGTCATC-3' and R, 5'-TCGTCATCGTCGAAATGGGC-3'; and *GAPDH* F, 5'-TGGTATGAGAGCTGGGGAATG-3'; and R, 5'-CCTCCCCACCTTGAAAGGAA-3').

In vitro vasculogenic mimicry assay. First, 50 µl thawed matrix gel solution (ABW Matrigel; cat. no. 082704; Shanghai Nova Medical Technology Co., Ltd.; http://www.abwbio.com/content/show/593/34) were evenly spread within each well of a 96-well plate. The plate was kept on ice for the duration of the experiment (4˚C; 30 min). Transfected CC and control CC cells ($3x10^4$) were dropped into the coagulated matrix glue. The plates were cultured at 37˚C, 5% CO_2 for 18 h to allow tuber formation. Images were captured at x4 magnification using a light microscope (IX53; Olympus Corporation). Image Pro (version 6.0; Media Cybernetics, Inc.) was used to calculate the number of branch points. Each experiment was performed in triplicate.

Migration and invasion assays. For migration assays, cells ($5.0x10^4$) were suspended in 300 µl serum-free medium and then seeded in the upper chamber of an 8-µm pore Transwell® insert (Corning, Inc.). Subsequently, 700 µl fresh medium with 10% FBS were added to the lower chamber of the Transwell insert and incubated for 24 h in a 37˚C incubator. For invasion assays, a 100 µl aliquot of Matrigel diluted 10-fold in PBS was added to the upper chamber of a Transwell insert and allowed to solidify for 10 min in a 37˚C incubator. cells ($1.0x10^5$) were suspended in 300 µl serum-free medium and then seeded in the upper chamber of an 8-µm pore Transwell® Matrigel insert (Corning, Inc.). Subsequently, 700 µl fresh medium with 10% FBS were added to the lower chamber of the Transwell insert and incubated for 24 h in a 37˚C incubator. After incubation for 24 h at 37˚C, the cells in the upper chamber were fixed with 4% paraformaldehyde for 2 h at RT and stained with 0.1% crystal violet for 1 h at RT. A light microscope used for observation of migratory/invasive cells in the lower chamber. The number of migrated cells were counted in 5 fields of view (original magnification, x10) using an Olympus IX53 microscope (Olympus Corporation).

Western blotting. After collecting and lysing the cells, the protein concentration in the soluble portion was determined using the BCA protein assay (cat. no. C0050; TargetMol Chemicals Inc.). The protein extraction buffer contained RIPA (cat. no. P0013B; Shanghai Beyotime Biotechnology Co., Ltd.), protease inhibitor cocktail (cat. no. C0001; TargetMol Chemicals Inc.) and PMSF (cat. no. ST506-2; Shanghai Beyotime Biotechnology Co., Ltd.). Equal amounts of protein (30 µg/lane) were separated using SDS-PAGE (10%) and then transferred to methanol-activated 0.45 µm PVDF membranes. The membranes were blocked with 5% milk at 20±5˚C for 1 h. The blocked membranes were incubated at 4˚C overnight with the following antibodies: A rabbit monoclonal anti-NSUN2 antibody (1:1,000; cat. no. AB259941; Abcam), a rabbit monoclonal anti-transfer RNA aspartic acid methyltransferase 1 (TRDMT1) antibody (1:1,000; cat. no. 19221-1-AP; Proteintech Group, Inc.; Wuhan Sanying Biotechnology), a rabbit polyclonal anti-MMP-9 antibody (1:1,000; cat. no. 10375-2-AP; Proteintech Group, Inc.; Wuhan Sanying Biotechnology), a rabbit polyclonal anti-aldehyde dehydrogenase 1 (ALDH1) antibody (1:1,000; cat. no. 15910-1-AP; Proteintech Group, Inc.; Wuhan Sanying Biotechnology), a rabbit polyclonal anti-ephrin type-A receptor 2 (EPHA2) antibody (1:1,000; cat. no. AF5238; Affinity Biosciences) and a rabbit polyclonal anti-GAPDH antibody (1:1,000; TA309157 OriGene Technologies, Inc.). Following extensive washing, the membranes were incubated at room temperature for 1 h with an HRP-conjugated sheep anti-rabbit secondary antibody (1:5,000; cat. no. A0208; Shanghai Beyotime Biotechnology Co., Ltd.). Following reaction with ECL reagent (cat. no. P0018S; Shanghai Beyotime Biotechnology Co., Ltd.), immunoreactive proteins bands were visualized using a Tanon™ 5200 chemiluminescence gel imaging system (Tanon Science and Technology Co., Ltd.). The results of the western blotting analyses were quantified using ImageJ (version 1.53; National Institutes of Health) and normalized to either the loading control or GAPDH.

Immunohistochemistry (IHC). The standard staining protocol in identifying VM is double staining with periodic acid-Schiff (PAS) and anti-CD31 antibodies (38,39). Tissue samples from patients with CC or paracancerous tissues and a CC tissue microarray (cat. no. HUteS140Su01; Shanghai Outdo Biotech

Co., Ltd) were fixed and then cut into 4 μm sections. Paraffin sections were dewaxed to water using a dewaxing agent (three baths of 10 min each), followed by gradient alcohol dehydration for 5 min per bath and finally rinsed thoroughly using distilled water. The blocking process was performed with 10% goat serum (cat. no. AR1009; Boster Biological Technology) at room temperature for 30 min. The tissue samples were treated with PH9.0 EDTA repair solution for antigen retrieval and then treated with a rabbit polyclonal anti-CD31 antibody (1:2,000; cat. no. AB76533; Abcam), a rabbit polyclonal anti-NSUN2 antibody (1:200; cat. no. AB259941; Abcam) or a rabbit polyclonal anti-MMP-9 antibody (1:200; cat. no. 10375-2-AP; Proteintech Group, Inc.; Wuhan Sanying Biotechnology). The sections were incubated overnight at 4˚C, washed and incubated with a secondary antibody. The secondary antibody used was goat anti-rabbit HRP (1:2,000; cat. no. ab205718; Abcam), incubated at 37˚C for 50 min. To perform PAS staining, the sections were first oxidized with periodic acid solution for 10 min, rinsed thoroughly with distilled water and blotted dry with absorbent paper. The sections were then stained with Schiff's reagent for 10-15 min and rinsed under running tap water for 10 min. The sections were then dehydrated through a graded series of ethanol (95% and absolute ethanol), cleared with a clearing agent and subsequently mounted. The stained sections were imaged using an optical microscope (original magnification, x20). The microarrays were scanned using the Hamamatsu NanoZoomer S360 (Hamamatsu Photonics K.K.). H&E staining was performed using reagents purchased from Hubei BIOSSCI Biotech Co., Ltd (cat. no. BP0211). The staining procedure was carried out as follows: Tissue sections were immersed in clearing solution for 10 min twice, with excess liquid gently shaken off between each step. Sections were rehydrated through a graded ethanol series: Absolute ethanol for 5 min, 95% ethanol for 5 min, 85% ethanol for 5 min and 75% ethanol for 5 min, followed by rinsing in distilled water for 1 min. Sections were stained with Harris hematoxylin solution for 4 min at room temperature and then rinsed under tap water for 2 min until no excess dye was released. Differentiation was performed using 0.8% hydrochloric acid alcohol for 2 sec, followed by rinsing with tap water. Sections were stained with alcohol-soluble eosin solution for 20 sec at room temperature without rinsing, then treated with 95% ethanol for 5 min and dehydrated via two changes of absolute ethanol (2 min each). Finally, sections were cleared in xylene and mounted with neutral balsam for microscopic examination.

Methylated RNA immunoprecipitation (IP). Total RNA was extracted from CC cell lines using TRIzol® reagent (Invitrogen; Thermo Fisher Scientific, Inc.). The RNA (each sample contained 300 μg of RNA, with a concentration of 1 μg/μl) was then fragmented at 94˚C for 5 min using fragmentation reagents (30 μl; cat. no. 3735438; Merck KGaA). After stopping the fragmentation process with stop buffer and vortexing, the RNA fragments were divided into two tubes, isolated by centrifugation and dissolved in 100 μl diethylpyrocarbonate (DEPC)-treated water. The RNA fragments were incubated with 10 μg antibodies against m^{5}C (cat. no. AB10805; Abcam) or 10 μg NSUN2 (cat. no. AB259941; Abcam) in methylated-RNA IP buffer (5X IP buffer with RNase inhibitor) for 4 h at 4˚C. 30 μl Protein A/G (cat. no. 3835713; Merck KGaA) magnetic beads were added and the mixture was incubated for an additional 4 h. The washing reagent used was IP Buffer (1X), prepared by diluting IP Buffer (5X) (cat. no. 3841555; Merck KGaA). Each complex was eluted with 100 μl of Elution Buffer (1X), which was prepared by combining 90 μl of IP Buffer (5X), 150 μl of m5C (20 mM stock; cat. no. 58366-64-6; Merck KGaA), 7 μl of RNase inhibitor and 203 μl of molecular biology-grade, RNase-free water. Subsequently, the complexes were further eluted with an additional 100 μl of 1X IP Buffer. The eluates were collected and precipitated by centrifugation at 15,000 x g for 30 min at 4˚C. The precipitate RNA was dissolved in an equal volume of DEPC-treated water and reversed transcribed into cDNA using the PrimeScript™ RT reagent Kit (Perfect Real Time) Kit (cat. no. RR037A; Takara Bio, Inc.). Quantitative PCR was used TB Green® Premix Ex Taq™ (Tli RNaseH Plus) (cat. no. RR420A; Takara Bio Inc.). The *MMP-9* mRNA IP assay primers used were as follows: 47-153 bp region F, 5'-GTG CTCCTGGTGCTGGGCTG-3' and R, 5'-GCCAGCTGCCTG TCGGTGAG-3'; 185-279 bp region F, 5'-CGGGTGGCA GAGATGCGTGG-3' and R, 5'-TCCAGCTCACCGGTCTCG GG-3'; 293-440 bp region F, 5'-AAGGCCATGCGAACCCCA CG-3' and R, 5'-AGGCGTCGTCAATCACCGCC-3'; 493-595 bp region F, 5'-CGTGTACAGCCGGGACGCAG-3' and R, 5'-AAAGGCGTGTGCCAGGAGCC-3'; 594-676 bp region F, 5'-TTTCCTCCTGGCCCCGGCAT-3' and R, 5'-TGGACC ACGACGCCCTTGC-3'; 730-842 bp region F, 5'-GGGCCG CTCCTACTCTGCCT-3' and R, 5'-TCTCGCTGGGGCAGA AGCCA-3'; 823-933 bp region F, 5'-TGGCTTCTGCCCCAG CGAGA-3' and R, 5'-TCCGTGGTGCAGGCGGAGTA-3'; 1070-1170 bp region F, 5'-TTCACTTTCCTGGGTAAG-3' and R, 5'-TTCTTGTCGCTGTCAAAG-3'; 1,261-1,390 bp region F, 5'-GCCGGAGGCGCTCATGTACC-3' and R, 5'-GGTGGT GGTTGGAGGCCGTG-3'; 1,565-1,651 bp region F, 5'-TGC AACGTGAACATCTTC-3' and R, 5'-CTCAGAGAATCG CCAGTA-3'; 1,869-2,004 bp region F, 5'-TCCGGAGTGGCA AGGGGAG-3' and R, 5'-TGCTGTCCAAAGGCACCCC-3'; 2,230-2,332 bp region F, 5'-TATTCTGTTCTGGAGGAA-3' and R, 5'-GGTTAGAGAATCCAAGTT-3'. The thermal cycling profile was as follows: Initial denaturation at 95˚C for 30 sec, followed by 55 cycles of at 95˚C for 5 sec and 60˚C for 30-34 sec (fluorescence data collection was performed at this step). Melt curve analysis was performed from 60-95˚C with a continuous fluorescence measurement at a ramp rate of 0.3˚C per sec. Analysis of relative gene expression data using real-time quantitative PCR and the $2^{-\Delta\Delta Ct}$ method and the input RNA as an internal control.

Dot blotting. Total RNA was incubated with oligo dT(25) beads (cat. no. S1550S; New England Biolabs, Inc.) for 10 min at RT and then washed with Lysis/Binding buffer (cat. no. B1556AVIAL; New England Biolabs, Inc.), Wash Buffer I (cat. no. B1558AVIAL; New England Biolabs, Inc.), Wash Buffer II (cat. no. B1559AVIAL; New England Biolabs, Inc.)and Low Salt Buffer (cat. no. B1557AVIAL; New England Biolabs, Inc.). The mRNA was eluted with Elution Buffer (cat. no. B1561AVIAL; New England Biolabs, Inc.) and samples containing 300 or 600 ng of mRNA were transferred to nylon membranes. The RNA was cross-linked under UV light (λ=254 nm) at 0.3 J/cm^2 and the membranes

were blocked with 5% skim milk in PBST for 1 h at RT. The membranes were incubated with anti-m^{5}C antibodies (1:1,000; cat. no. AB10805; Abcam) overnight at 4˚C, washed extensively with PBST (0.1% Tween) and then incubated with an HRP-conjugated sheep anti-mouse secondary antibody (1:5,000; cat. no. AF2819; Shanghai Beyotime Biotechnology Co., Ltd.) for 2 h at RT. The membranes were washed with PBST (0.1% Tween) and then stained with methylene blue. The nylon membranes containing the target mRNA were visualized using a Tanon™ 5200 chemiluminescence gel imaging system (Tanon Science and Technology Co., Ltd.)

RNA stability assay. CC cells were cultured in 6-well plates overnight and then treated with 5 μg/ml actinomycin D (cat. no. HY-17559; MedChemExpress) for 3, 6 or 9 h at 37˚C. Total RNA was then extracted using TRIzol® reagent (Invitrogen; Thermo Fisher Scientific, Inc.) RNA was reverse transcribed into cDNA using the PrimeScript™ RT reagent Kit (Perfect Real Time) Kit (cat. no. RR037A; Takara Bio, Inc.) according to the manufacturer's protocol and the DNA was stored at -20˚C. Quantitative PCR was performed on an ABI StepOne Plus Real-Time PCR System (Applied Biosystems; Thermo Fisher Scientific, Inc.) with three replicates for each sample, using TB Green® Premix Ex Taq™ (Tli RNaseH Plus) (cat. no. RR420A; Takara Bio Inc.). Analysis of relative gene expression data using RT-qPCR as aforementioned and data were analyzed using the comparative Cq method. Levels of gene expression were normalized to that of *GAPDH*. The mRNA half-life time was estimated using linear regression analysis.

CC data acquisition and statistical analysis. RNA-sequencing data and corresponding clinical information for cervical squamous cell carcinoma and endocervical adenocarcinoma (CESC) were downloaded from The Cancer Genome Atlas (TCGA) database via the Genomic Data Commons (GDC) data portal (https://portal.gdc.cancer.gov/). Gene expression profiles that were normalized using fragments per kilobase million (FPKM) were obtained for subsequent analysis, while clinical data including survival time and survival. A comprehensive list of VM-promoting factors (Myc, Sox2, POU5F1, SNAIL family members, ZEB2, TWIST, MMP-2, MMP-9, and MMP-14) and 5-methylcytosine (m5C) RNA methylation-related genes was compiled through literature review and publicly available databases. The m5C-related genes primarily included 'writers' (methyltransferases such as NSUN family members and TRDMT1), 'readers' (YBX1, ALYREF), and 'erasers' (TET family members). Expression profiles of these VM-promoting factors and m5C-related genes were extracted from the FPKM expression matrix for further analysis. Student's t-test was performed to evaluate the differential expression of VM-promoting factors and m5C-related genes between tumor and normal tissues, with a P-value of <0.05 considered statistically significant. For survival analysis, patients were stratified into high- and low-expression groups based on the median expression value of each VM-promoting factor and m5C-related gene. Kaplan-Meier survival curves were generated to assess the association between gene expression levels and overall survival (OS), and the log-rank test was employed to determine statistical significance between survival curves. Hazard ratios (HR) and 95% confidence intervals (CI) were calculated using Cox proportional hazards regression models. All statistical analyses were conducted using R software (version 4.2.1; Posit Software, PBC), with the 'survival' (version 3.8.2; https://github.com/therneau/survival) and 'survminer' (version 0.5.0; https://rpkgs.datanovia.com/survminer/index.html) packages utilized for survival analysis and visualization. All tests were two-sided, and P-values <0.05 were considered statistically significant.

Statistical analysis. Data are presented as mean ± SD from at least three independent biological replicates. For comparisons between paired samples (tumor vs. adjacent normal tissue), statistical significance was assessed using a paired two-tailed Student's t-test when data passed normality (Shapiro-Wilk test) and homogeneity of variance assumptions. For comparisons between two independent groups, statistical significance was determined using an unpaired two-tailed Student's t-test for data that passed both normality (assessed by the Shapiro-Wilk test) and homogeneity of variance tests. For data that did not meet the assumptions for parametric testing, a two-tailed Mann-Whitney U test was employed For comparisons among ≥3 groups, one-way ANOVA followed by Tukey's post hoc test was performed. Linear relationships between variables were assessed through Pearson's correlation analysis and linear regression. Survival analysis was carried out using the Kaplan-Meier method, and differences between groups were compared with the log-rank test. P<0.05 was considered to indicate a statistically significant difference. Statistical analyses were performed using GraphPad Prism (version 7; Dotmatics).

Results

Vasculogenic mimicry is increased in CC and is associated with poor prognosis. In order to explore the prevalence of VM in CC, three pairs of CC and paracancerous tissues from human subjects were selected for IHC staining using the diagnostic standard of CD31/PAS double staining (Fig. 1A). Among the three pairs of tissue samples, VM was only revealed to exist in CC tissues and not in paracancerous tissues and VM was increased in CC tissues. To study the impact of VM on CC prognosis, a CC tissue microarray was first analyzed by IHC staining and then the results were subjected to a double-blind statistical comparison to the prognoses of the subjects (Fig. 1B). VM-positivity was revealed to be associated with shorter biochemical progression-free survival after surgery (P=0.004; Kaplan-Meier analysis) (Fig. 1C; P<0.01). These results suggest that VM exists at higher levels in CC tissues and that its presence is associated with a poor prognosis.

MMP-9, a key Vasculogenic mimicry-promoting factor, is highly expressed in CC and is associated with poor prognosis. In order to further explore the association of VM with CC, a CC database from TCGA was used to analyze the expression levels of >12 key factors affecting the three steps that lead to VM generation: CSC formation, EET and ECM reconstruction (Fig. 2A). The genes encoding SRY-box transcription factor 2 (*Sox2*) and *MMP-9* were revealed to be highly expressed in CC (Fig. 2A). Further analysis of the impact of these two

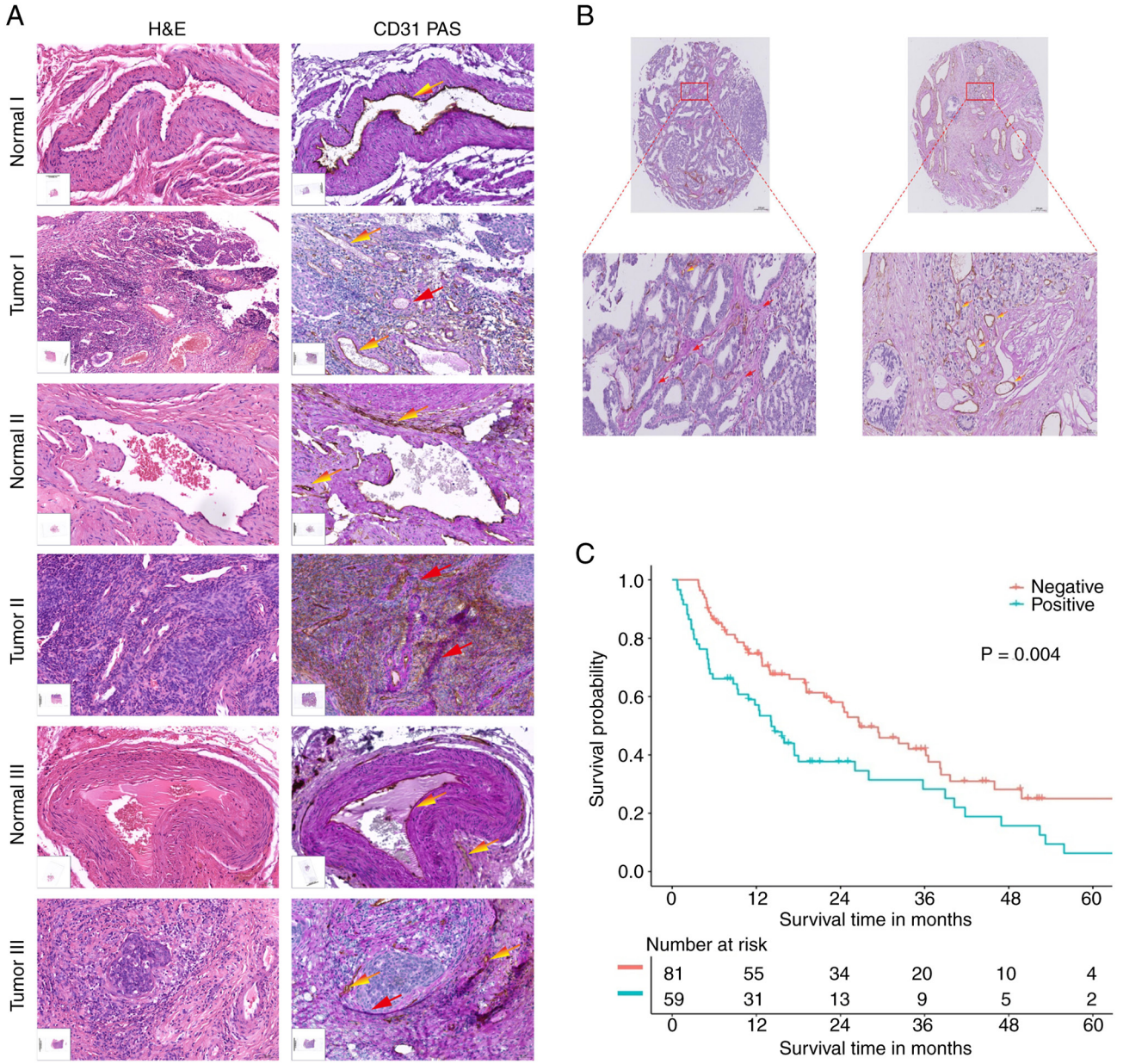

Figure 1. Vasculogenic mimicry is increased in cervical cancer and is associated with poor prognosis. (A) Three pairs of CC and paracancerous tissues were analyzed by H&E and PAS staining and immunohistochemical detection of CD31, with $CD31^-/PAS^+$ serving as the diagnostic standard for VM. Red arrows indicate VM and yellow arrows indicate endothelial angiogenesis. Scale bar, 50 mm. Original magnification, x20. (B) A CC tissue microarray, consisting of tissues from 140 cases of CC, was subjected to CD31/PAS analysis. Red arrows indicate VM and gold arrows indicate endothelial angiogenesis. Original magnification, x20. (C) Level of VM positivity was compared with patient outcomes in the form of biochemical progression-free survival (P=0.004, log-rank test). PAS, periodic acid-Schiff; VM, vasculogenic mimicry; CC, cervical cancer.

factors on the prognosis of CC demonstrated that patients with CC exhibiting higher *MMP-9* expression levels tend to have a poorer prognosis, while those with higher *Sox2* expression levels generally experience an improved prognosis (Fig. 2B and C).

Similarly, IHC staining of 20 pairs of CC and paracancerous tissue samples demonstrated that the protein levels of MMP-9 were significantly higher in cancerous tissues compared with paired normal tissues (P<0.001) (Fig. 2D and E). The expression levels of *MMP-9* mRNA was further analyzed using RT-qPCR of 44 pairs of samples. The present study identified that *MMP-9* mRNA was significantly highly expressed in cancerous tissues compared with paired normal tissues (P<0.01) (Fig. 2F and G).

To further study the potential role of MMP-9 in promoting VM in CC, VM-competent CC cell lines were subjected to hypoxic stimulation. HeLa and SiHa cells were induced in a 0.1% O_2 incubator (40-42) and proteins collected at 24, 48 and 72 h were analyzed using western blotting (Fig. 2H). The level of ALDH1, a key factor affecting VM through the CSC pathway, was revealed to be slightly increased under continuous hypoxia, although the increase did not rise to the level of statistical significance (P<0.05) (43,44). The level of EPHA2, a key factor affecting VM through the EET pathway (45,46), was revealed to be decreased. By contrast, the level of MMP-9, a key factor affecting VM through the ECM pathway, increased over time and the

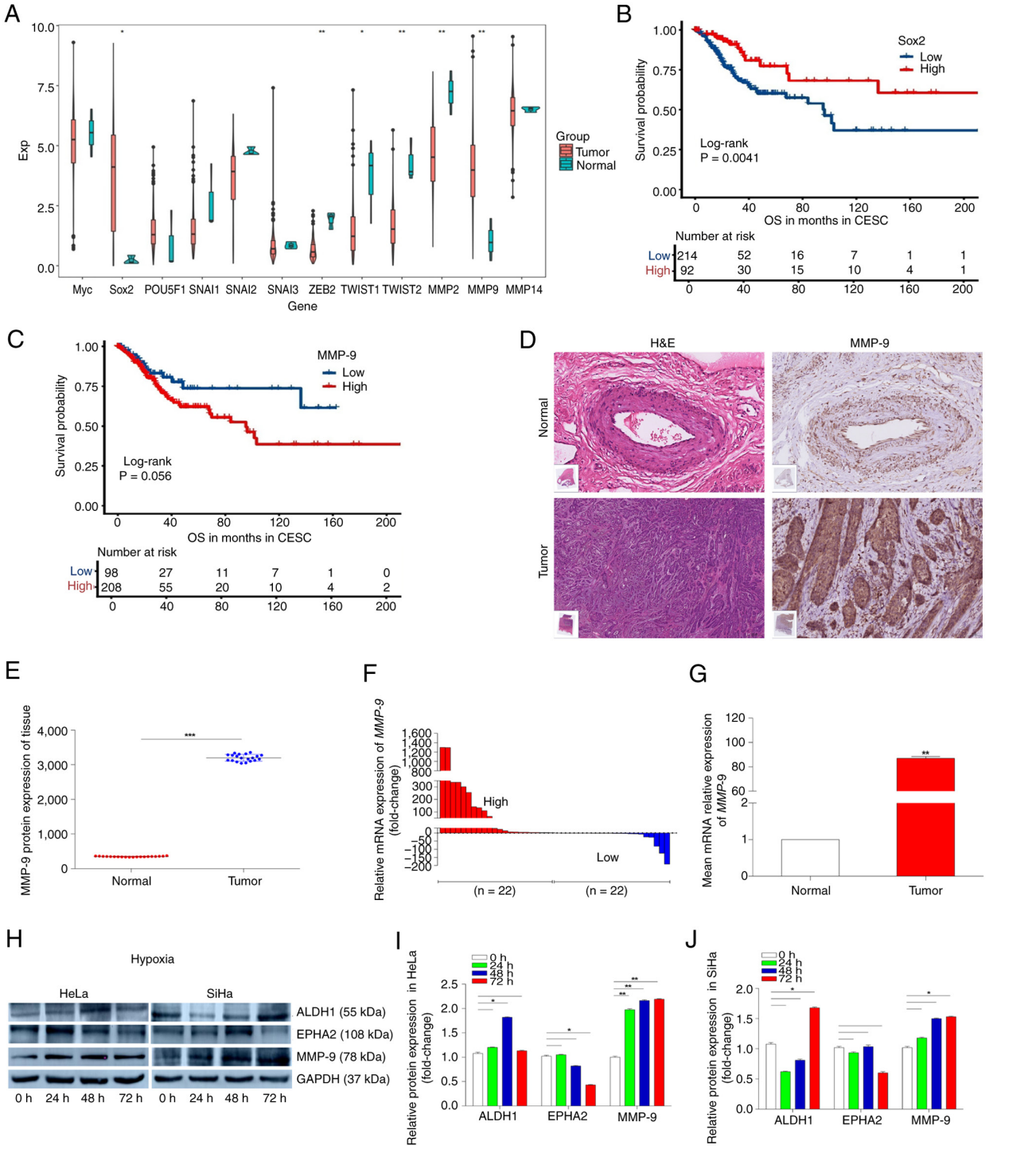

Figure 2. *MMP-9*, a factor that promotes Vasculogenic mimicry, is highly expressed in CC and is associated with poor prognosis. (A) CC database of TCGA was used to analyze key factors associated with VM. (B) Association of *Sox2* expression with overall survival in CC (log-rank test). (C) Association of *MMP-9* expression with overall survival in CC (log-rank test). (D) Panoramic scans after immunohistochemical detection of MMP-9 and H&E staining in samples from cancerous and paracancerous tissues from subjects with CC. Scale bar, 50 μm. Original magnification, x20. (E) Protein levels of MMP-9 in 20 paired samples, with the MMP-9 level in CC tissue expressed compared with that in the paired normal tissue. (F) Expression levels of *MMP-9* mRNA in 44 paired CC and paracancerous tissues, with *MMP-9* expression in CC tissue expressed compared with that in the paired normal tissue. (G) Comparison of the average expression levels of *MMP-9* mRNA in CC tissues compared with paracancerous tissues. (H) HeLa and SiHa cells were incubated under hypoxia (0.1% O_2) and proteins collected at 24, 48 and 72 h for western blotting of ALDH1, EPHA2, MMP-9 and GAPDH. ImageJ was used to semi-quantify western blotting signals from HeLa (I) and SiHa (J) cells. GAPDH served as an internal reference. *P<0.05, **P<0.01 and ***P<0.001. MMP-9, matrix metalloproteinase 9; VM, vasculogenic mimicry; ALDH1, aldehyde dehydrogenase 1; EPHA2, ephrin type-A receptor 2; TCGA, The Cancer Genome Atlas; Sox2, SRY-box transcription factor 2; CC, cervical cancer; CESC, cervical squamous cell carcinoma.

level of MMP-9 at 72 h was significantly higher compared with in non-hypoxic cells (P<0.01) (Fig. 2I and J). These results suggest that compared with the CSC pathway, the effect of VM generation on CC mainly depends on the ECM remodeling pathway and the increased expression levels of MMP-9 may serve a key role.

m^{5}C methyltransferase NSUN2 is upregulated in CC and is associated with poor prognosis. Next, the mechanism by which MMP-9 levels are increased in VM in the context of CC were investigated. A dot blot test demonstrated that the m^{5}C methylation modification was significantly increased upon hypoxic induction of VM-competent HeLa (P<0.001) and SiHa (P<0.01) cells (Fig. 3A-C). Therefore, TCGA CC database was then used to analyze the expression levels of all enzymes that generate the m^{5}C modification. The present study identified a high expression level of *NSUN2* and low expression level of *TRDMT1* (which encodes transfer RNA aspartic acid methyltransferase 1) among the methyltransferases (Fig. 3D).

To investigate the impact of hypoxia on the levels of these proteins, VM-competent HeLa and SiHa cells were induced in a 0.1% O_2 incubator and proteins collected at 24, 48 and 72 h were analyzed using western blotting. The expression levels of NSUN2 (P<0.05) were consistently high under continuous hypoxia, while the expression levels of TRDMT1 were not significantly changed and was even slightly downregulated. Therefore, the present study concluded that NSUN2 is a key methyltransferase in the VM process under these conditions (Fig. 3E-G).

Regarding human tissue samples, *NSUN2* mRNA expression was revealed to be higher in CC tissue samples compared with in normal control samples (Fig. 3H). Similarly, a quantitative analysis of 44 pairs of CC and paracancerous tissue samples demonstrated that *NSUN2* mRNA levels were significantly higher in CC tissues compared with paracancerous tissues (P<0.001) (Fig. 3I) and IHC analyses of 20 pairs of samples revealed that expression was also significantly higher at the protein level (P<0.001) (Fig. 3J and K).

Notably, the level of *NSUN2* expression in CC was associated with a poor prognosis in the form of biochemical progression-free survival (P=0.018; log-rank test; Fig. 3L). These results suggest that m^{5}C methylation of RNA increases in VM-competent CC cells under hypoxic conditions and that the methyltransferase NSUN2 serves a key role in this process.

NUSN2 promotes vasculogenic mimicry, invasion and migration of CC cells. As NSUN2 was a key candidate for the direct mediator of increased m^{5}C methylation in hypoxic CC cells, the potential impact of this methyltransferase on the VM process. First, *in vitro* experiments were performed in order to explore whether NSUN2 can promote VM in CC cells. Preliminary experiments involved the normal cervical cell line HaCaT and the CC cell lines HeLa, SiHa, CaSki, C33A and HT-3. According to RT-qPCR analyses, *NSUN2* was revealed to be most significantly highly expressed in HeLa (P<0.001) and SiHa (P<0.01) cells (Fig. 4A); therefore, these two CC cell lines were selected for further analyses.

Plasmids were designed to produce shRNA to interfere with expression levels of *NSUN2*. Following transfection of these plasmids and a control plasmid into HeLa and SiHa cells, the cells were subjected to hypoxic conditions for 24 h and RNA was collected for RT-qPCR analyses. Compared with the control group, the level of *NSUN2* mRNA was significantly decreased in cells transfected with NSUN2-interfering plasmids, particularly with plasmid shNUSN2-3 (P<0.001) (Fig. 4B). Notably, the level of *MMP-9* mRNA was also significantly decreased in cells transfected with shNUSN2-3 (P<0.01) (Fig. 4C).

To further investigate whether NSUN2 serves a key role in the methylation modification and thus the level of m^{5}C, cells transfected with the interfering plasmid were subjected to hypoxia and the mRNA was subjected to dot blotting. The present study identified that the level of m^{5}C was significantly reduced in HeLa (P<0.001)and SiHa (P<0.01) cells and this effect was particularly strong in HeLa cells (Fig. 4D-F). The results suggest that NSUN2 serves a key role in m^{5}C methylation modification in CC.

The levels of NSUN2 and MMP-9 proteins were also investigated under these conditions. After transfection of the *NSUN2*-interfering plasmid into HeLa and SiHa cells and subjection to hypoxic conditions for 48 h, proteins were collected and analyzed using western blotting. Compared with the control, transfection of *NSUN2*-interfering plasmids led to significant decreases in the levels of NSUN2 protein, particularly with the shNUSN2-3 plasmid (P<0.001) (Fig. 4G and H). The level of MMP-9 protein was also significantly decreased upon interference with *NUSN2* expression (P<0.001) (Fig. 4I).

The effects of *NSUN2* knockdown on the two-dimensional tube formation that characterizes VM were investigated under hypoxic conditions. After *NSUN2* knockdown, the tube formation ability of HeLa and SiHa cells was significantly decreased (P<0.01); however, overexpression of *MMP-9* significantly reversed this effect of *NSUN2* knockdown on cell tube formation (P<0.001) (Fig. 4J and K). Similarly, both invasion and migration abilities of HeLa and SiHa cells under hypoxic conditions were significantly diminished after *NSUN2* knockdown (P<0.01); however, overexpression of *MMP-9* significantly reversed these effects (P<0.001) (Fig. 4L-O). These results suggest that NSUN2 is required for generation of VM of CC cells and they demonstrate that NSUN2 promotes the invasion and migration of CC cells under hypoxic conditions. It was also identified that MMP-9 is a potential downstream mediator of these effects of NSUN2.

NSUN2 maintains the stability of MMP-9 mRNA. Because MMP-9 was revealed to be a potential downstream mediator of the effects of NSUN2, the present study further investigated the relationships between these two factors. First, a Pearson's correlation analysis of the levels of *NSUN2* and *MMP-9* mRNA in 44 pairs of CC tissue samples was performed. The levels of *NSUN2* mRNA was revealed to be significantly positively correlated with the level of *MMP-9* mRNA (P<0.0001; Fig. 5A). In addition, methylated-RNA immunoprecipitation assays demonstrated a marked enrichment of m^{5}C in *MMP-9* mRNA in HeLa and SiHa cells in two regions: Between nucleotides 1,070 and 1,170 and between nucleotides 1,565 and 1,651 (Fig. 5B and C). Similarly, RNA immunoprecipitation assays indicated that NSUN2 was highly enriched on *MMP-9* mRNA within the 1,565-1,651 region in both HeLa and SiHa cells (Fig. 5D and E).

The present study also identified that in HeLa and SiHa cells, the stability of *MMP-9* mRNA markedly decreased upon transfection of an *NSUN2*-interference plasmid and the stability markedly increased upon overexpression of *NSUN2* (Fig. 5F and G). These results were consistent with a model in which NUSN2 modifies *MMP-9* mRNA in the region of 1,565 to 1,651 bp and thus, that MMP-9 is a downstream mediator of the effects of NUSN2 on the hypoxic VM response in CC

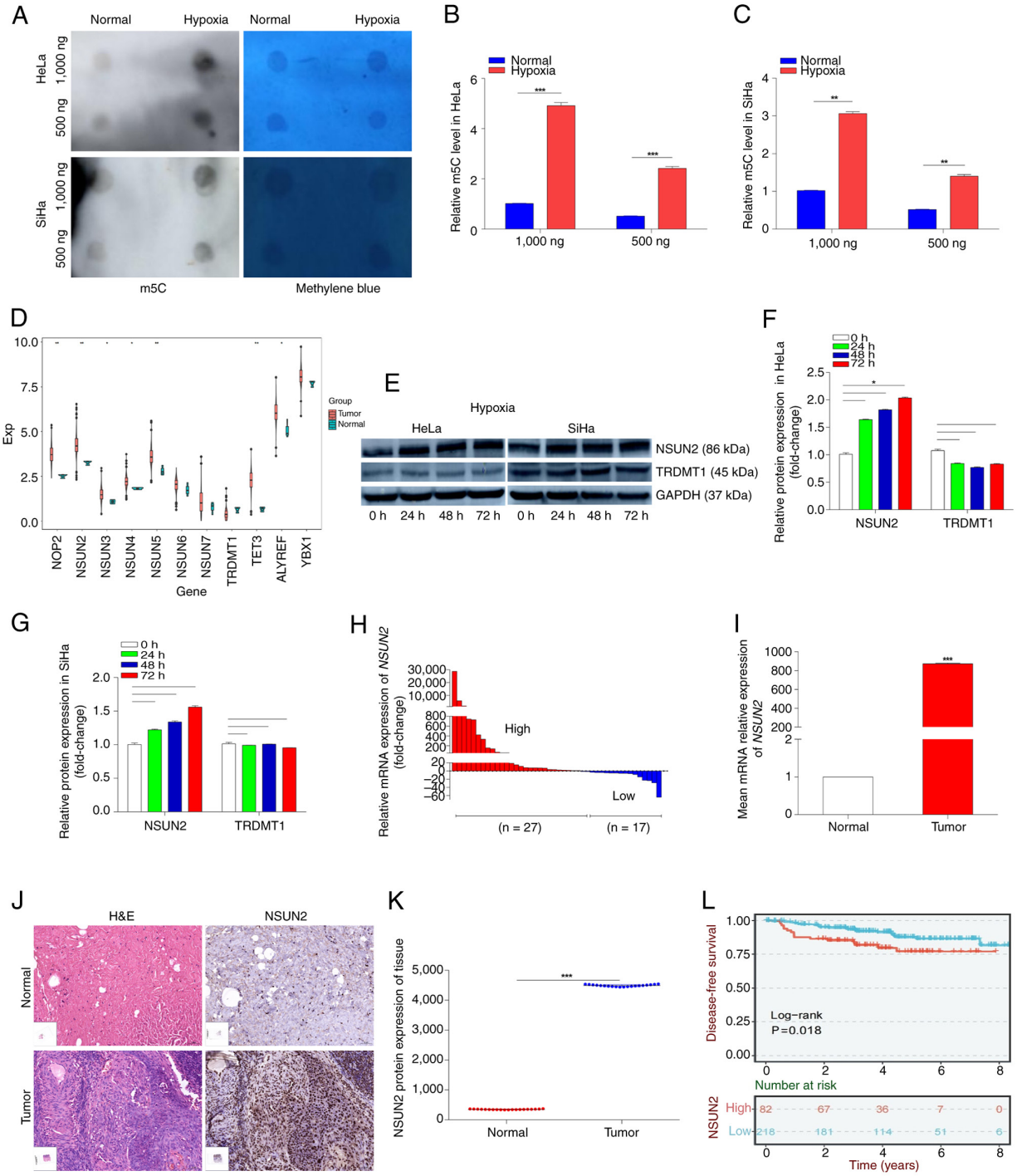

Figure 3. m^{5}C RNA methyltransferase NUSN2 is significantly upregulated in CC and its gene expression is associated with poor prognosis. (A) The level of m^{5}C modification of RNA in CC cells was analyzed using a dot blot assay. Methylene blue staining served as an internal reference. (B) Semi-quantitative analysis of dot blot results in HeLa cells. (C) Semi-quantitative analysis of dot blot results in SiHa cells. (D) Expression levels of genes encoding m^{5}C methyltransferases was analyzed within a CC database of TCGA. (E) HeLa and SiHa cells were incubated under hypoxia (0.1% O_2) and proteins collected at 24, 48 and 72 h were analyzed for NSUN2, TRDMT1 and GAPDH by western blotting. ImageJ was used to quantify western blotting signals from (F) HeLa and (G) SiHa cells. GAPDH served as an internal reference. (H) mRNA expression level of *NSUN2* in 44 pairs of CC and paracancerous tissues were quantified using RT-qPCR. Gene expression in cancer tissues is expressed compared with expression in normal tissues. (I) Comparison of the average expression level of *NSUN2* mRNA in CC tissues compared with paracancerous tissues. (J) Panoramic scans after IHC detection of NSUN2 and H&E staining in CC and paracancerous tissues. Scale bar, 50 μm. Magnification, x20. (K) Protein levels of NSUN2 in 20 paired CC and paracancerous tissues, with the NSUN2 level in CC tissue expressed compared with that in the paired normal tissue. (L) Level of *NSUN2* expression in CC was associated with a poor prognosis in the form of biochemical progression-free survival (P=0.018; log-rank test). *P<0.05, **P<0.01 and ***P<0.001. MMP9, matrix metalloproteinase 9; VM, vasculogenic mimicry; CC, cervical cancer; IHC, immunohistochemistry; NSUN2, NOP2/Sun RNA methyltransferase 2; m^{5}C, 5-methylcytidine; TRDMT1, transfer RNA aspartic acid methyltransferase 1; TCGA, The Cancer Genome Atlas; RT-qPCR, reverse transcription-quantitative PCR; IHC, immunohistochemistry.

cells. In this model, NSUN2 increases the expression levels of MMP-9 by maintaining the stability of the *MMP-9* mRNA, leading to the promotion of VM generation by CC cells and enhanced malignant progression (Fig. 5H).

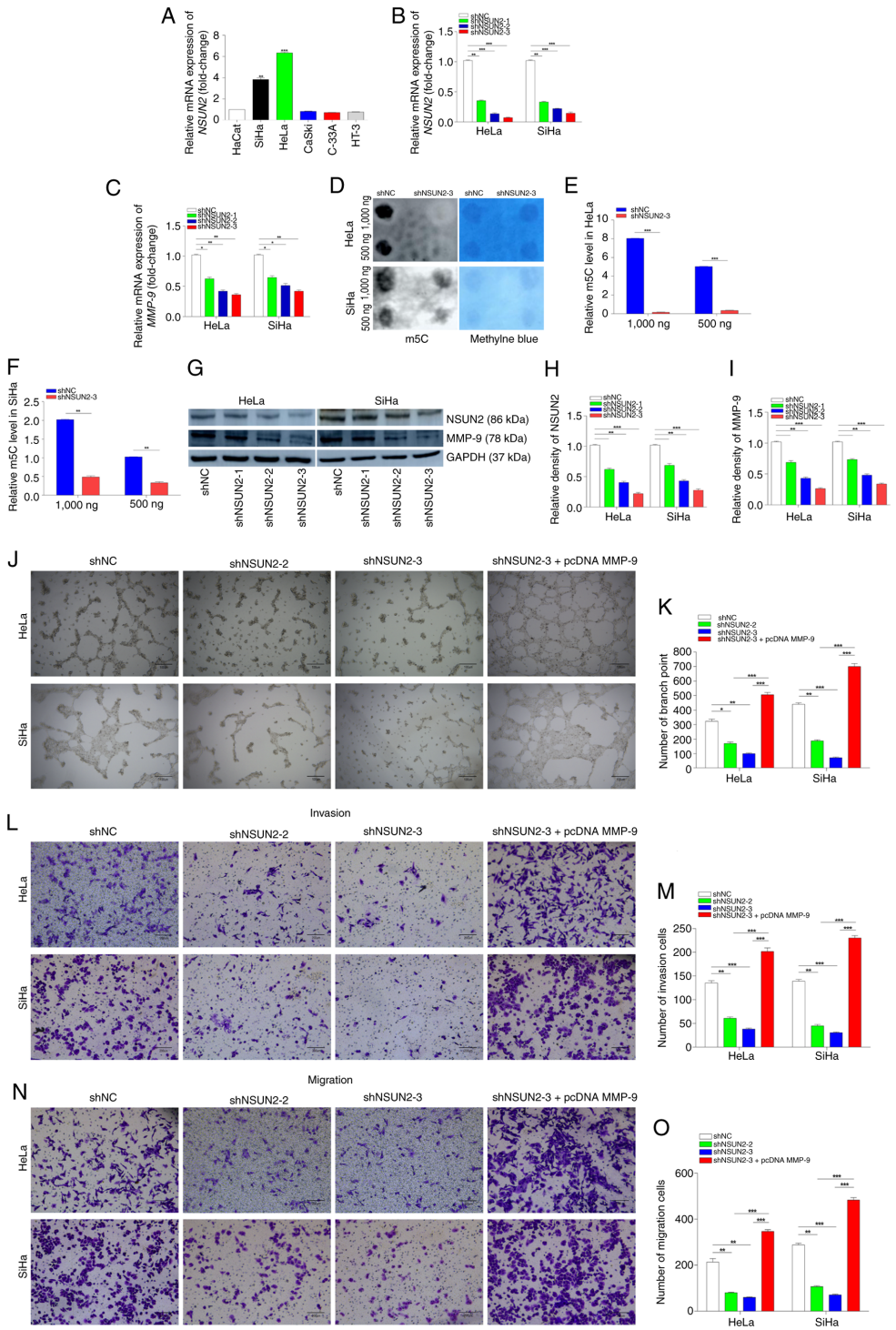

Figure 4. NSUN2 promotes Vasculogenic mimicry, invasion and migration of CC cells under hypoxic conditions. (A) Expression levels of *NSUN2* in CC cells lines (HeLa, SiHa, CaSki, C33A and HT-3) and in a normal cervical cell line (HaCaT). (B) RT-qPCR was used to determine relative expression levels of *NSUN2* mRNA in HeLa and SiHa cells after transfection of shRNAs and incubation under hypoxia for 24 h. (C) Relative expression levels of *MMP-9* mRNA in HeLa and SiHa cells transfected with the *NSUN2*-interfering plasmid and incubated under hypoxia for 24 h. (D) Dot blot assay analysis of m^{5}C expression levels in HeLa and SiHa cells after 48 h of hypoxia culture following transfection with *NSUN2* knockdown plasmids. (E) Semi-quantitative analysis of dot blot results in HeLa cells. (F) Semi-quantitative analysis of dot blot results in SiHa cells. (G) Western blotting was used to investigate NSUN2 and MMP-9 protein levels in HeLa and SiHa cells transfected with the *NSUN2*-interfering plasmid and incubated under hypoxia for 48 h. ImageJ was used to semi-quantify western blotting bands for (H) NSUN2 and (I) MMP-9 protein levels. (J) 2D tube-forming assays of HeLa and SiHa cells transfected with an *NSUN2*-interfering plasmid and incubated under hypoxia. Scale bar, 100 μm. Original magnification, x4. (K) Assay displayed in panel (J) was quantified using Image Pro. (L) Invasion assay of HeLa and SiHa cells transfected with a control plasmid, shNSUN2-2 or shNSUN2-3 or with shNSUN2 and pcDNA MMP-9. Scale bar, 200 μm. Original magnification, x10. (M) Assay displayed in panel was quantified using Image Pro. (N) Migration assay of HeLa and SiHa cells transfected with a control plasmid, shNSUN2-2 or shNSUN2-3 or with shNSUN2 and pcDNA MMP-9. Scale bar, 200 μm. Original magnification, x10. (O) Assay displayed in panel (N) was quantified using Image Pro. *P<0.05, **P<0.01 and ***P<0.001. VM, Vasculogenic mimicry; CC, cervical cancer; IHC, immunohistochemistry; NSUN2, NOP2/Sun RNA methyltransferase 2; m^{5}C, 5-methylcytidine; RT-qPCR, reverse transcription-quantitative PCR; IHC, immunohistochemistry; CaSki, human cervical cancer cell line with intestinal metastasis; C33A, human cervical cancer cell line; HaCaT, human skin keratinocytes cell line; HeLa, human cervical cancer cell line; HT-3, human cervical cancer cell line; MMP9, matrix metalloproteinase 9; SiHa, human cervical squamous cell line; pcDNA, plasmid cloning DNA; shRNA, short hairpin RNA; NC, negative control.

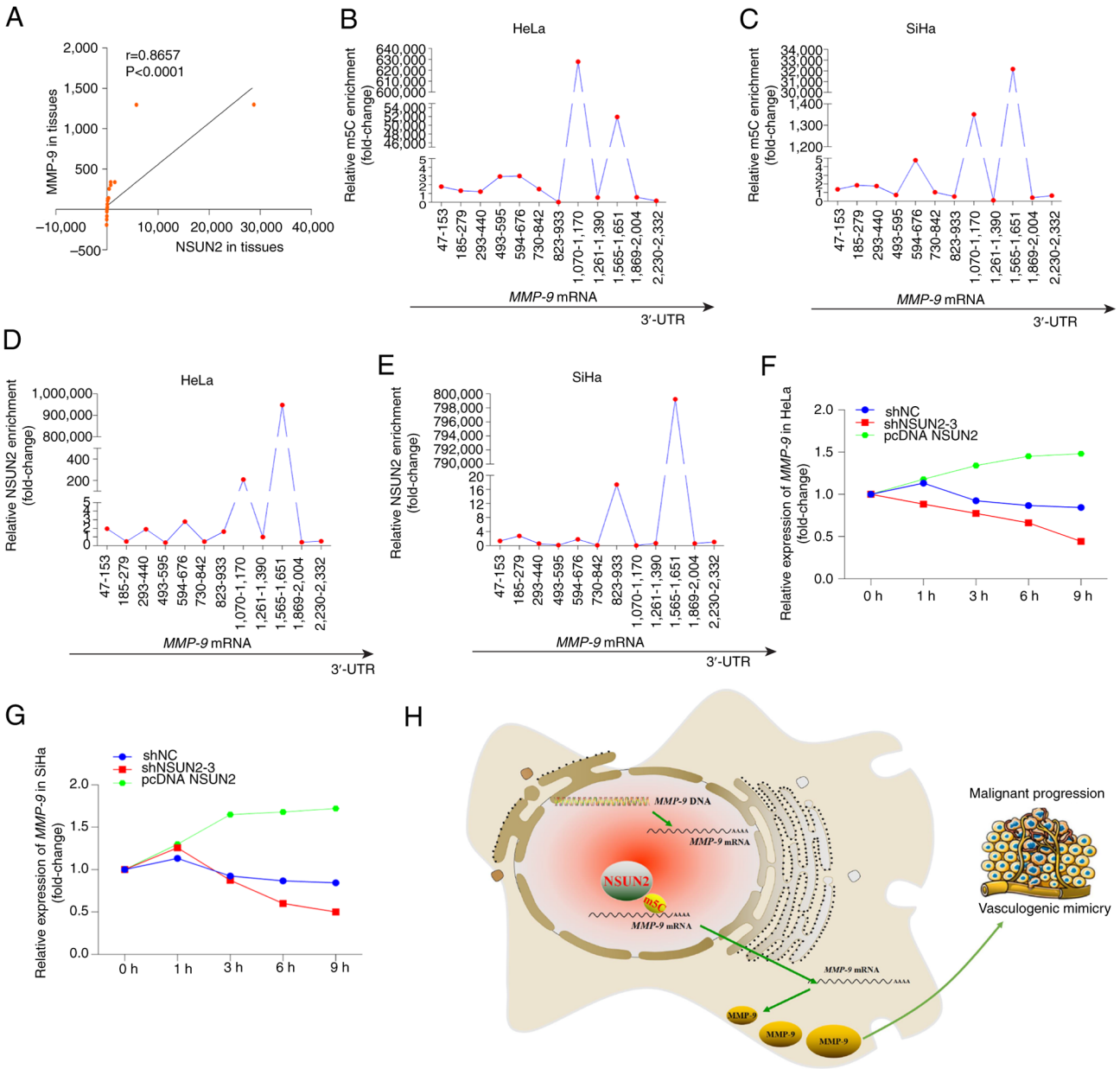

Figure 5. NSUN2 increases the stability of *MMP-9* mRNA. (A) A positive correlation was observed between *NSUN2* and *MMP-9* mRNA expression levels in 44 pairs of samples from subjects with CC. Enrichment of the m^5C modification of *MMP-9* mRNA in HeLa (B) and SiHa (C) Cells were measured with anti-m^5C methylated-RNA IP assays. Interaction of NSUN2 with *MMP-9* mRNA in (D) HeLa and (E) SiHa cells was measured with anti-*NSUN2* RNA IP assays. Stability of *MMP-9* mRNA after interference with and overexpression of NSUN2 was measured in (F) HeLa and (G) SiHa cells. (H) A model illustrating the proposed mechanism by which NSUN2-mediated stabilization of *MMP-9* mRNA promotes Vasculogenic mimicry in CC. NSUN2, NOP2/Sun RNA methyltransferase 2; m^5C, 5-methylcytidine; pcDNA, plasmid cloning DNA; shRNA, short hairpin RNA; HeLa, human cervical cancer cell line; MMP9, matrix metalloproteinase 9; SiHa, human cervical squamous cell line; IP, immunoprecipitation; CC, cervical cancer; NC, negative control.

Discussion

Globally, CC accounted for about 7.7% of all female cancer deaths globally, making it one of the deadliest cancers for women, with ~348,000 deaths annually. (1). While radiation therapy and radical surgery can improve the 5-year survival rate for patients with early-stage CC (47,48), there is an urgent need to explore novel strategies for the treatment of distant metastases and drug resistance for patients with advanced CC. Neovascularization is a potential vulnerability in advanced cancer, as when the diameter of a tumor >2 mm, the inner cells become starved for oxygen and nutrients and new blood vessels are needed. Therefore, tumor cells secrete a large number of vascular growth factors, such as VEGF and FGF-2, to promote the formation of blood vessels around the tumor.

Certain cancer cells mimic endothelial cells and align along a deposited basement membrane to form lumenized, interconnecting vessel-like structures that perfuse blood and fuse to the endothelium, in a process called VM (49). Tumor cells that shed from VM ducts are more likely to undergo early tumor metastasis to distal organs through the VM-dependent vasculature and endothelium-dependent vessels (38,39). In the hypoxic tumor microenvironment, tumor cells that have the ability to engage in VM typically revert to a poorly

differentiated state, thus forming CSCs, which tend to be resistant to chemotherapy agents (4,5). Therefore, it is key to study VM to develop novel strategies for the treatment of metastasis and drug resistance in advanced CC and exploring the molecular mechanisms underlying VM in CC may provide a theoretical basis for novel tools to diagnose and treat CC in the future.

Notably, the present study provides further evidence that VM influences the invasiveness and metastatic potential of malignant tumors and that VM status might serve as an independent tool to evaluate prognoses in CC and other cancer types.

In the hypoxic tumor microenvironment, the VM process involves CSC, EET or ECM, but the specific mechanism leading to VM in CC remained unclear. In the present study, the statuses of key factors affecting CSC, EET and ECM in CC were analyzed using a CC database in TGCA and the results suggested that *Sox2*, which affects CSC and *MMP-9*, and thus the ECM, were highly expressed in CC. However, the present analysis also demonstrated that only *MMP-9* expression was associated with poor prognosis in CC; therefore, the present study performed further analysis of MMP-9. Experimentally, the present study identified that expression levels of *MMP-9* were increased at both the mRNA and protein levels in CC tissues compared with paracancerous normal tissues. VM-competent CC cell lines (HeLa and SiHa) were selected to explore the possible mechanisms that influence the formation of VM under hypoxic conditions. Notably, hypoxic induction led to an increase in the levels of MMP-9, a protein that influences the ECM pathway in the process of VM. By contrast, the levels of ALDH1, which affects the CSC pathway were revealed to increase only slightly under continuous hypoxia and EPHA2, which affects the EET pathway, was revealed to be decreased. These results provided further evidence that increased VM in CC is mainly dependent on the ECM pathway and that MMP-9 serves a key role. Notably, MMP-9 expression was elevated in CC and hypoxia-induced conditions, with MMP-mediated degradation serving a pivotal role in CC metastatic progression.

Next, the mechanisms by which the levels of MMP-9 increase in this context were considered. Various tumor cells, including CC (50), pancreatic cancer (51), glioma (52), breast cancer (53) and liver cancer (54), have been revealed to undergo changes to RNA methylation under hypoxic conditions. The present study specifically focused on the RNA modification m^{5}C, which has gained notable attention at the frontiers of epigenomics research. Roles for this modification in promoting proliferation, migration, angiogenesis and drug resistance have been reported in multiple tumor types (such as NSCLC, bladder cancer and glioma) (32-34). In the present study, the results of a dot blot assay revealed that the levels of the m^{5}C modification increased significantly in the RNA of VM-competent HeLa and SiHa cells under hypoxic conditions. TCGA CC database further indicated that the methyltransferase *NSUN2* is significantly upregulated in CC. In order to determine if NSUN2 might be responsible for the changes to the m^{5}C modification, the proteins in VM-competent HeLa and SiHa cells under continuous hypoxia were analyzed using western blotting. The results suggested that compared with methyltransferase TRDMT1, the protein level of NSUN2 continued to increase with the time of hypoxia induction, in accordance with the increasing m^{5}C levels under these same conditions. By contrast, when the levels of *NSUN2* were decreased using shRNA, the levels of m^{5}C were significantly decreased. Therefore, the present study concluded that NSUN2 serves a key role in establishing the m^{5}C methylation modification in CC. Subsequently, the present study identified that NSUN2 levels are significantly higher in CC and that high expression level of the *NSUN2* gene is associated with a poor prognosis in CC. These results suggest that NSUN2 might contribute to the malignant progression of CC by influencing the VM process.

Subsequently, the present study performed further analysis of the model in which NUSN2 contributes to VM generation and thus to invasion and migration of CC. Interfering with the expression of *NUSN2* using a shRNA-expressing plasmid system inhibited the VM process as well as invasion and migration of HeLa and SiHa cells. Notably, the present study also observed that decreasing the levels of *NSUN2* was associated with decreased expression of *MMP-9* at the mRNA and protein levels; accordingly, overexpression of *MMP-9* significantly reversed the inhibitory effects of *NSUN2* knockdown on VM generation, invasion and migration. Therefore, these results indicated that *NSUN2* may act as an oncogene, as its increased expression promotes VM and malignant progression of CC by increasing the expression levels of MMP-9.

The m^{5}C modulation alters gene expression at the post-transcriptional level by affecting RNA stability. Therefore, we hypothesized that NSUN2 might interact with and modify *MMP-9* mRNA. This potential relationship between NSUN2 and *MMP-9* mRNA was investigated by focusing on the m^{5}C modifications within this mRNA. The present study identified that *MMP-9* mRNA is markedly enriched in m^{5}C in two regions of the mRNA: Between nucleotides 1,070 and 1,170 and between nucleotides 1,565 and 1,651. Further investigation in the present study demonstrated that NSUN2 formed a stable interaction with *MMP-9* mRNA within the region from nucleotides 1,565-1,651, suggesting that NSUN2 might modify and thus stabilize *MMP-9* mRNA. Subsequently, the stability of *MMP-9* mRNA was revealed to decrease upon shRNA-mediated interference of *NSUN2* expression and increase upon overexpression of *NSUN2*. Therefore, the effect of NSUN2 on VM generation in CC is likely mediated at least in part by increasing levels of MMP-9. Thus, the present study enhances current understanding of the VM process during the malignant progression of CC and provides insights into the regulation of VM by the m^{5}C RNA modification. It also suggests that VM, NSUN2 and MMP-9 are potentially valuable targets in the treatment of solid tumors in the future.

Future research should address the limitations of the present study to further validate the findings. While th present work establishes a novel link between NSUN2, m5C modification of MMP9 mRNA and VM in CC, the enzymatic activity of the upregulated MMP-9 protein was not assessed. Therefore, subsequent investigation will be to determine if increased expression translates to heightened proteolytic function using activity-based assays. This would provide a more robust foundation for evaluating repurposed drugs such as the MMP inhibitor doxycycline (which shows anti-VM efficacy in other types of cancer) (55,56), within the present experimental model. Additionally, the specific molecular interplay, including

whether m5C readers such as YBX1 (32,57-59) are involved in conveying the NSUN2-mediated effect, remains an open and mechanistically important avenue for future research.

The present study demonstrated that NUSN2 influences the cellular level of MMP-9 by stabilizing its mRNA. If NUSN2 expression increases, its effect on MMP-9 promotes malignant progression of CC by enhancing VM. These results indicate that both NSUN2 and MMP-9 may serve as biomarkers for early diagnosis and prognosis in CC and these two enzymes may serve as targets for novel anti-vascular therapies in the future.

Acknowledgements

Not applicable.

Funding

No funding was received.

Availability of data and materials

The data generated in the present study may be requested from the corresponding author.

Authors' contributions

JL and HS conceptualized and designed the present study. MY, KS and GL provided study materials, recruited patients, were involved in the interpretation of the clinical data and contributed to the critical revision of the manuscript for important intellectual conten. XX, LQ and MQ collected and assembled the data. JH, XX and MQ conducted data analysis and interpreted the data. JL wrote the manuscript. JL and HS confirmed the authenticity of all the raw data. All authors have read and approved the final manuscript.

Ethics approval and consent to participate

The present study was approved by the Ethics Committee of Nanjing Medical University [approval no. (2024) Court Ethics Opinion No. 028-1; Nanjing, China] and written informed consent was obtained from all participants.

Patient consent for publication

Not applicable.

Competing interests

The authors declare that they have no competing interests.

References

1. Bray F, Laversanne M, Sung HY, Ferlay J, Siegel RL, Soerjomataram I and Jemal A: Global cancer statistics 2022: GLOBOCAN estimates of incidence and mortality worldwide for 36 cancers in 185 countries. CA Cancer J Clin 74: 229-263, 2024.
2. Zhou M, Gao Y, Zhang Y, He L, Gao B, Zhang Y, Claret FX, Calin GA and Wang D: CircZFR/YTHDF3 axis drives lymph node metastasis in cervical cancer via FASN translation. Mol Cancer 24: 218, 2025.
3. Zhang C, Yuan L, Wen W, Shao C, Liao Y, Jia Y, Zhao X, Liao Y, Xu D, Chen L, *et al*: LNMAC promotes cervical squamous cell carcinoma lymphatic metastasis via epigenetic regulation of FGF2-induced Lymphangiogenesis. Adv Sci (Weinh) 11: e2404645, 2024.
4. Hyeon DY, Nam D, Shin HJ, Jeong J, Jung E, Cho SY, Shin DH, Ku JL, Baek HJ, Yoo CW, *et al*: Proteogenomic characterization of molecular and cellular targets for treatment-resistant subtypes in locally advanced cervical cancers. Mol Cancer 24: 77, 2025.
5. Cao G, Wang Y, Zeng H, Zhi Y, Guo Y, Xu M, Ruan Y, Wang Y, Xiao Y, Lu J, *et al*: Oligoclonal tumor-specific CD8 T-cell revival and IRE1α/XBP1-GDF15-mediated immunosuppressive niches determine neoadjuvant chemoimmunotherapy efficacy in cervical cancer. J Immunother Cancer 13: e012630, 2025.
6. Maniotis AJ, Folberg R, Hess A, Seftor EA, Gardner LM, Pe'er J, Trent JM, Meltzer PS and Hendrix MJ: Vascular channel formation by human melanoma cells in vivo and in vitro: Vasculogenic mimicry. Am J Pathol 155: 739-752, 1999.
7. Harris AL: Hypoxia-a key regulatory factor in tumour growth. Nat Rev Cancer 2: 38-47, 2002.
8. Sun B, Zhang D, Zhao N and Zhao X: Epithelial-to-endothelial transition and cancer stem cells: Two cornerstones of vasculogenic mimicry in malignant tumors. Oncotarget 8: 30502-30510, 2017.
9. Zhao B, Wu M, Hu Z, Ma Y, Wang Q, Zhang Y, Li Y, Yu M, Wang H and Mo W: Thrombin is a therapeutic target for non-small-cell lung cancer to inhibit vasculogenic mimicry formation. Signal Transduct Target Ther 5: 117, 2020.
10. Huang M, Lin Y, Wang C, Deng L, Chen M, Assaraf YG, Chen ZS, Ye W and Zhang D: New insights into antiangiogenic therapy resistance in cancer: Mechanisms and therapeutic aspects. Drug Resist Updat 64: 100849, 2022.
11. Yeh YH, Hsiao HF, Yeh YC, Chen TW and Li TK: Inflammatory interferon activates HIF-1α-mediated epithelial-to-mesenchymal transition via PI3K/AKT/mTOR pathway. J Exp Clin Cancer Res 37: 70, 2018.
12. He M, Yang H, Shi H, Hu Y, Chang C, Liu S and Yeh S: Sunitinib increases the cancer stem cells and vasculogenic mimicry formation via modulating the lncRNA-ECVSR/ERβ/Hif2-α signaling. Cancer Lett 524: 15-28, 2022.
13. Lacal PM, Atzori MG, Ruffini F, Scimeca M, Bonanno E, Cicconi R, Mattei M, Bernardini R, D'Atri S, Tentori L and Graziani G: Targeting the vascular endothelial growth factor receptor-1 by the monoclonal antibody D16F7 to increase the activity of immune checkpoint inhibitors against cutaneous melanoma. Pharmacol Res 159: 104957, 2020.
14. Yu P, Han Y, Meng L, Tian Y, Jin Z, Luo J, Han C, Xu W, Kong L and Zhang C: Exosomes derived from pulmonary metastatic sites enhance osteosarcoma lung metastasis by transferring the miR-194/215 cluster targeting MARCKS. Acta Pharm Sin B 14: 2039-2056, 2024.
15. Wang Q, Huang Y, Jiang M, Tang Y, Wang Q, Bai L, Yu C, Yang X, Ding K, Wang W, *et al*: The demethylase ALKBH5 mediates ZKSCAN3 expression through the m6A modification to activate VEGFA transcription and thus participates in MNNG-induced gastric cancer progression. J Hazard Mater 473: 134690, 2024.
16. Zhang R, Zhang D, Han F, Song X, Zhang Y, Zhang J, Zhu Q and Qin Y: The deubiquitinase USP7 and E3 ligase TRIM21 regulate vasculogenic mimicry and malignant progression of RMS by balancing SNAI2 homeostasis. J Exp Clin Cancer Res 43: 135, 2024.
17. Huang XY, Huang ZL, Huang J, Xu B, Huang XY, Xu YH, Zhou J and Tang ZY: Exosomal circRNA-100338 promotes hepatocellular carcinoma metastasis via enhancing invasiveness and angiogenesis. J Exp Clin Cancer Res 39: 20, 2020.
18. Liu Y, Tang R, Cao Y, Wu N, Qin Q, Chen Y, Wei X, Ren J, Sun Y, Zhou H, *et al*: LIFU/MMP-2 dual-responsive release of repurposed drug disulfiram from nanodroplets for inhibiting vasculogenic mimicry and lung metastasis in triple-negative breast cancer. J Nanobiotechnology 22: 209, 2024.
19. Shirakawa K, Kobayashi H, Heike Y, Kawamoto S, Brechbiel MW, Kasumi F, Iwanaga T, Konishi F, Terada M and Wakasugi H: Hemodynam-ics in vasculogenic mimicry and angiogenesis of infammatory breast cancer xenograft. Cancer Res 62: 560-566, 2002.
20. Baeten CIM, Hillen F, Pauwels P, de Bruine AP and Baeten CGMI: Prognostic role of vasculogenic mimicry in colorectal cancer. Dis Colon Rectum 52: 2028-2035, 2009.

21. Liu R, Yang K, Meng C, Zhang Z and Xu Y: Vasculogenic mimicry is a marker of poor prognosis in prostate cancer. Cancer Biol Ther 13: 527-533, 2012.
22. Liu WB, Xu GL, Jia WD, Li JS, Ma JL, Chen K, Wang ZH, Ge YS, Ren WH, Yu JH, *et al:* Prognostic signifcance and mechanisms of patterned matrix vasculogenic mimicry in hepatocellular carcinoma. Med Oncol 28 (Suppl 1): S228-S238, 2011.
23. Ding J, Jia X, Zuo B, He J, Yang J and He Y: A novel monoclonal antibody targeting a novel epitope of VE-cadherin inhibits vasculogenic mimicry of lung cancer cells. Oncol Rep 39: 2837-2844, 2018.
24. Tang HS, Feng YJ and Yao LQ: Angiogenesis, vasculogenesis, and vasculogenic mimicry in ovarian cancer. Int J Gynecol Cancer 19: 605-610, 2009.
25. Guo QJ, Yuan Y, Jin ZC, Xu T, Gao YB, Wei HM, Li CH, Hou W and Hua BJ: Association between tumor vasculogenic mimicry and the poor prognosis of gastric cancer in China: An updated systematic review and meta-analysis. Biomed Res Int 2016: 2408645, 2016.
26. Fujimoto A, Onodera H, Mori A, Nagayama S, Yonenaga Y and Tachibana T: Tumour plasticity and extravascular circulation in ECV304 human bladder carcinoma cells. Anticancer Res 26: 59-69, 2006.
27. Sun B, Zhang D, Zhang S, Zhang W, Guo H and Zhao X: Hypoxia influences vasculogenic mimicry channel formation and tumor invasion-related protein expression in melanoma. Cancer Lett 249: 188-197, 2007.
28. Qie S, Sun BC, Zhao XL, Zhang SW, Sun T, Gao SY and Wang XH: Correlation between expressions of matrix metalloproteinase-2& 9 and vasculogenic mimicry in gastrointestinal stromal tumors. ZhonghuaYi Xue Za Zhi 89: 1106-1109, 2009 (In Chinese).
29. Boccaletto P, Machnicka MA, Purta E, Piatkowski P, Baginski B, Wirecki TK, de Crécy-Lagard V, Ross R, Limbach PA, Kotter A, *et al*: MODOMICS: A database of RNA modification pathways. 2017 update. Nucleic Acids Res 46: D303-D307, 2018.
30. García-Vílchez R, Sevilla A and Blanco S: Post-transcriptional regulation by cytosine-5 methylation of RNA. Biochim Biophys Acta Gene Regul Mech 1862: 240-252, 2019.
31. Chen YS, Yang WL, Zhao YL and Yang YG: Dynamic transcriptomic m5 C and its regulatory role in RNA processing. Wiley Interdiscip Rev RNA 12: e1639, 2021.
32. Wang YQ, Wei JY, Feng LY, Li OW, Huang L, Zhou SX, Xu YJ, An K, Zhang Y, Chen RY, *et al*: Aberrant m5C hypermethylation mediates intrinsic resistance to gefitinib through the NSUN2/YBX1/QSOX1 axis in EGFR-mutant non-small-cell lung cancer. Mol Cancer 22: 81, 2023.
33. Wang N, Chen RX, Deng MH, Wei WS, Zhou ZH, Ning K, Li YH, Li XD, Ye YL, Wen JH, *et al*: m5C-dependent cross-regulation between nuclear reader ALYREF and writer NSUN2 promotes urothelial bladder cancer malignancy through facilitating RABL6/TK1 mRNAs splicing and stabilization. Cell Death Dis 14: 139, 2023.
34. Pan A, Xue Y, Ruan X, Dong W, Wang D, Liu Y, Liu L, Lin Y, Tiange E, Lin H, *et al*: m5C modification of LINC00324 promotes angiogenesis in glioma through the CBX3/VEGFR2 pathway. Int J Biol Macromol 257: 128409, 2024.
35. Wang L, Zhang J, Su Y, Maimaitiyiming Y, Yang S, Shen Z, Lin S, Shen S, Zhan G, Wang F, *et al*: Distinct roles of m5C RNA methyltransferase NSUN2 in major gynecologic cancers. Front Oncol 25: 786266, 2022.
36. Chen YJ, Zuo XZ, Wei QL, Xu J, Liu XY, Liu SL, Wang HC, Luo QY, Wang YY, Yang Y, *et al*: Upregulation of LRRC m5C modification-mediated mRNA stability suppresses apoptosis and facilitates tumorigenesis in cervical cancer. Int J Biol Sci 19: 691-704, 2023.
37. Livak KJ and Schmittgen TD: Analysis of relative gene expression data using real-time quantitative PCR and the 2(-Delta Delta C(T)) method. Methods 25: 402-408, 2001.
38. Pearsall SM, Williamson SC, Humphrey S, Hughes E, Morgan D, Marqués FJ, Awanis G, Carroll R, Burks L, Shue YT, *et al*: Lineage plasticity in SCLC generates non-neuroendocrine cells primed for vasculogenic mimicry. J Thorac Oncol 18: 1362-1385, 2023.
39. Treps L, Faire S and Clere N: Vasculogenic mimicry, a complex and devious process favoring tumorigenesis-Interest in making it a therapeutic target. Pharmacol Ther 223: 107805, 2021.
40. Tomita H, Tanaka K, Tanaka T and Hara A: Aldehyde dehydrogenase 1A1 in stem cells and cancer. Oncotarget 7: 11018-11032, 2016.
41. Bhattacharya S, Calar K and de la Puente P: Mimicking tumor hypoxia and tumor-immune interactions employing three-dimensional in vitro models. J Exp Clin Cancer Res 39: 75, 2020.
42. Samuel T, Rapic S, O'Brien C, Edson M, Zhong Y and DaCosta RS: Quantitative intravital imaging for real-time monitoring of pancreatic tumor cell hypoxia and stroma in an orthotopic mouse model. Sci Adv 9: eade8672, 2023.
43. Brown BA, Myers PJ, Adair SJ, Pitarresi JR, Sah-Teli SK, Campbell LA, Hart WS, Barbeau MC, Leong K, Seyler N, *et al*: A histone methylation-MAPK signaling axis drives durable epithelial-mesenchymal transition in hypoxic pancreatic cancer. Cancer Res 84: 1764-1780, 2024
44. Sun HZ, Yao N, Cheng SQ, Li LQ, Liu SQ, Yang Z, Shang GJ, Zhang DF and Yao Z: Cancer stem-like cells directly participate in vasculogenic mimicry channels in triple-negative breast cancer. Cancer Biol Med 16: 299-311, 2019.
45. Liu X, He H, Zhang F, Hu X, Bi F, Li K, Yu H, Zhao Y, Teng X, Li J, *et al*: m6A methylated EphA2 and VEGFA through IGF2BP2/3 regulation promotes vasculogenic mimicry in colorectal cancer via PI3K/AKT and ERK1/2 signaling. Cell Death Dis 13: 483, 2022.
46. Ju RJ, Li XT, Shi JF, Li XY, Sun MG, Zeng F, Zhou J, Liu L, Zhang CX, Zhao WY and Lu WL: Liposomes, modified with PTD(HIV-1) peptide, containing epirubicin and celecoxib, to target vasculogenic mimicry channels in invasive breast cancer. Biomaterials 35: 7610-7621, 2014.
47. Landoni F, Maneo A, Colombo A, Placa F, Milani R, Perego P, Favini G, Ferri L and Mangioni C: Randomized study of radical surgery versus radiotherapy for stage Ib-IIa cervical cancer. Lancet 350: 535-540, 1997.
48. Quinn MA, Benedet JL, Odicino F, Maisonneuve P, Beller U, Creasman WT, Heintz APM, Ngan HYS and Pecorelli S: Carcinoma of the cervix uteri. FIGO 26th annual report on the results of treatment in gynecological cancer. Int J Gynaecol Obstet 95: S43-S103, 2006.
49. Tan LY, Cockshell MP, Moore E, Min KKM, Ortiz M, Johan MZ, Ebert B, Ruszkiewicz A, Brown MP, Ebert LM and Bonder CS: Vasculogenic mimicry structures in melanoma support the recruitment of monocytes. Oncoimmunology 11: 2043673, 2022.
50. Liang L, Zhu Y, Li J, Zeng J and Wu L: ALKBH5-mediated m6A modification of circCCDC134 facilitates cervical cancer metastasis by enhancing HIF1A transcription. J Exp Clin Cancer Res 41: 261, 2022.
51. Wirth M and Schneider G: A hypoxia-epigenetics axis drives EMT in pancreatic cancer. Cancer Res 84: 1739-1741, 2024.
52. Guo XF, Qiu W, Li B, Qi YH, Wang SB, Zhao RR, Cheng B, Han X, Du H, Pan ZW, *et al*: Hypoxia-induced neuronal activity in glioma patients polarizes microglia by potentiating RNA m6A demethylation. Clin Cancer Res 30: 1160-1174, 2024.
53. Xiong JJ, Zhou ZR, Jiang YL, Li QF, Geng ZH, Guo JH, Yan CJ and Zhang J: Hypoxic stabilization of RIPOR3 mRNA via METTL3-mediated m6A methylation drives breast cancer progression and metastasis. Oncogene 43: 3426-3441, 2024.
54. Zhang Q, Wei T, Yan LS, Zhu SQ, Jin W, Bai Y, Zeng YD, Zhang XF, Yin ZX, Yang JL, *et al*: Hypoxia-Responsive lncRNA AC115619 encodes a micropeptide that suppresses m6A modifications and hepatocellular carcinoma progression. Cancer Res 83: 2496-2512, 2023.
55. Meng J, Sun B, Zhao XL, Zhang D, Zhao XM, Gu Q, Dong XY, Zhao N, Liu PM and Liu YR: Doxycycline as an inhibitor of the epithelial-to-mesenchymal transition and vasculogenic mimicry in hepatocellular carcinoma. Mol Cancer Ther 13: 3107-3122, 2014.
56. Sun B, Zhang S, Zhang D, Yin X, Wang S, Gu Y and Wang Y: Doxycycline influences microcirculation patterns in B16 melanoma. Exp Biol Med (Maywood) 232: 1300-1307, 2007.
57. Liu XY, Wei QL, Yang CY, Zhao HY, Xu J, Mobet Y, Luo QY, Yang D, Zuo XZ, Chen NX, *et al*: RNA m5C modification upregulates E2F1 expression in a manner dependent on YBX1 phase separation and promotes tumor progression in ovarian cancer. Exp Mol Med 56: 600-615, 2024.
58. Zhang YY, Li CT, Zhou YJ, Li H, Li J, Xiong QP, Zhou W, Huang W, Zhang QFC, Xiang YF, *et al*: A cohort of mRNAs undergo high-stoichiometry NSUN6-mediated site-specific m5C modification. Nat Commun 16: 6119, 2025.
59. Shaw A, Ajit K, Chataignier M and Gullerova M: Non-coding Y RNA fragments in a complex with YBX1 modulate PARP1 residency at DNA double strand breaks. Nucleic Acids Res 53: gkaf517, 2025.